Analogous Saturation Mechanisms of the Ion and Electron Temperature Gradient Drift Wave Turbulence

V. Sokolov and A. K. Sen

Phys. Rev. Lett. **113**, 095001 — Published 25 August 2014

DOI: 10.1103/PhysRevLett.113.095001

Analogous saturation mechanisms of the ion and electron temperature gradient drift wave turbulence.

V. Sokolov and A. K. Sen

Plasma Research Laboratory, Columbia University, New York, New York 10027

Abstract

New experimental results and theoretical arguments indicate that a novel saturation mechanism of the electron temperature gradient (ETG) modes is related to its coupling to a damped ion acoustic (IA) mode. The experimental bi-coherence data show multimode coupling between two high frequency radial harmonics of ETG in the vicinity of (~2MHz) and one low frequency IA (~45kHz) mode. A unique feedback diagnostic also verifies this coupling. It is pointed out that a near identical mechanism is responsible for ITG mode saturation [V.Sokolov, and A.K. Sen, Phys. Rev. Lett. 92, 165002 (2004)], indicating its plausible generic nature.

PACS numbers: 52.35.Kt, 52.35.Mw

The turbulent thermal transport is a fundamental open physics issue in fusion science. The most plausible physics scenario for this anomalous ion and electron transport appears to be based on drift modes: Ion Temperature Gradient (ITG) and Electron Temperature Gradient (ETG) instabilities [1-3].

Ion turbulent transport is fairly understood. Extensive theoretical and simulation work clearly establish both ion and electron dynamic behaviors, both linear and nonlinear [4-12].In contrast, experimental validation of theories of electron transport is lacking. The number of experiments about identifications of ETG mode and consequent electron transport is very limited [13-16] due to certain diagnostic problems with the high frequency and short wavelengths of electron turbulence.

We experimentally investigate the novel saturation mechanism of ITG modes in a series of basic experiments in Columbia Linear Machine (CLM) [17,18]. This mechanism was explained by an unique 3-wave coupling of two ITG radial harmonics due to profile variation of ω_T^* [19] and an ion acoustic wave (IA): $\omega_{ITG,l=0} - \omega_{ITG,l=1} \Rightarrow \omega_{IA}$ [17,18]. We also experimentally studied complimentary roles of IA damping and zonal flows (ZF)[20] shearing in the saturation of ITG [21]. The stabilizing effect of ZF on the parent ITG modes via flow shear appears to be small [22]. Now we report experimental results and theoretical estimation of nonlinear saturation mechanism of the ETG modes.

The layout of CLM has been described in Ref. [23,24]. CLM is steady-state collisionless cylindrical plasma machine with an uniform axial magnetic field (Fig.1). The typical plasma parameters in CLM are: $n \sim 5\times10^9 cm^{-3}$, $B \approx 0.1T$, $T_e \approx 5-20eV$, and $T_i \approx 5eV$, the diameter d ~ 6cm and plasma column length L ~ 150cm, respectively [24]. One needs a strong radial electron temperature gradient to cause an ETG mode.

Toward this end the electrons of the plasma core are effectively heated via parallel acceleration by a positively biased (+20V) disk mesh (See Fig.1.). The moderate neutral pressure in the transition region guarantees that the accelerated electrons are thermalized to a Maxwellian distribution. Production and identification of slab ETG mode have been successfully demonstrated in a basic experiment in Columbia Linear Machine (CLM) [24]. This result has been recently validated by numerical simulation [25]. The first experimental scaling of electron thermal transport coefficient vs amplitude of ETG mode was also obtained [26].

We now study the nonlinear saturation mechanism of ETG modes. We present the experimental evidence of the coupling of ETG modes and a low frequency mode through experimental bi-coherence data. The low frequency mode is identified as ion acoustic mode leading to a 3-wave coupling model of two high frequency radial harmonics of ETG modes and one low frequency ion acoustic mode. This has been verified by a novel feedback diagnostic.

Figure 2 shows the typical power spectra of plasma potential fluctuations. The mode with frequency f ~ 2 MHz has been identified as an ETG mode with azimuthal wave number *m~11–13,* $k_\perp \rho_e << 1$, $k_\perp \rho_i > 1$ and propagating in the electron diamagnetic direction. The characteristic of the drift waves, $k_{//} << k_\perp$, is also satisfied by this mode [24]. The mode with frequency f ~ 140 kHz has been identified as an $\vec{E} \times \vec{B}$ mode with azimuthal mode number m =1, $k_{//} = 0$, always present in CLM [24]. Note also the presence of low frequency fluctuations f ~ 45 kHz identified as IA mode and as described below.

It is noted that in CLM (as well as in tokamaks), the mode frequency is Doppler shifted by the equilibrium $\vec{E}\times\vec{B}$ rotation of the plasma column with frequency $\omega_E = (m/r)\cdot V_{ExB}$, where m is azimuthal mode number. In this experiment m was about 11-13. From this it follows that the Doppler shift frequency ω_E also obeys the selection rule of 3-wave resonant mode coupling:

$$m_1(\mathbf{k}_1) \pm m_2(\mathbf{k}_2) = m_3(\mathbf{k}_3),\ \ \omega_{E1}\pm\omega_{E2}=\omega_{E3}$$

It is well known that the presence of 3-wave coupling can be determined via bi-spectrum [27]. The normalized autobispectrum, called the autobicoherency is defined as:

$$b^2(\omega_1,\omega_2) = \frac{\left|\left\langle X(\omega_1)X(\omega_2)X^*(\omega_1+\omega_2)\right\rangle\right|^2}{\left\langle\left|X(\omega_1)X(\omega_2)\right|^2\right\rangle\left\langle\left|X(\omega_1+\omega_2)\right|^2\right\rangle} \quad ,$$

where $X(\omega_i)$ are Fourier amplitudes.

Fig.3a. shows a typical bicoherence and the corresponding power spectrum. In the bicoherence figures the X and Y axis are ω_1 and ω_2 respectively, both are in units of kHz/2π. We note that the dense patches of contours on the diagonal in ω_1- ω_2 plane represent self-coupling of modes, while the off-diagonal patches indicate cross-coupling of modes. The bicoherence corresponding to cross-coupling between ETG mode ω_1 and low frequency $\omega_2 \sim 2\pi\cdot 45$ kHz mode is seen Fig.3a as a horizontal patch and dense horizontal contours in Fig 3b; the value of bicoherence is $b^2 \sim 0.1$. This may indicate mode coupling between one low frequency mode $\omega_2 \sim 2\pi\cdot$ 45 kHz, which is visible in the low frequency end of the power spectrum (See Fig.2.) and two higher frequency radial harmonics, $\omega_1=\omega_{12\_1}$(m=12, *l*=1) $\sim 2\pi\cdot$ 1.85 MHz , $\omega_3 =\omega_{12\_0}$(m=12, *l*=0)) $\sim 2\pi\cdot$ 1.9 MHz of ETG modes. Therefore, this can be considered as multimode interaction leading to saturation via the damped ion acoustic mode. Here *m*, *l* refer to azimuthal and radial harmonic mode numbers, respectively as described below.

Parenthetically, we tried to directly drive a pure IA mode via appropriately biased ring probe (See Fig.1.) in the absence of drift wave turbulence. We found this was not possible, presumably due to its strong damping [28].

It is noted that two weak patches with $\omega_2 \sim 2\pi\cdot 140$ kHz in Fig.3. correspond 3 wave coupling of two ETG modes and ExB mode. The right weak patch is $\omega_{ETG,m=12} + \omega_{ExB,m=1} \Rightarrow \omega_{ETG,m=13}$ and left patch is $\omega_{ETG,m=11} + \omega_{ExB,m=1} \Rightarrow \omega_{ETG,m=12}$.

The solution of fluid eigenmode equation for slab ITG mode with non-uniform temperature gradient profiles [18,19] yields its radial harmonics. Fig.4. shows the radial profiles of the electron temperature and the inverse temperature scale length $\left(L_{Te}(r)\right)^{-1} = -d(\ln T_e)/dr$. Using isomorphism of electron and ion response we can obtain the same fluid eigenmode equation [18,19,29] for ETG mode with non-uniform $\omega_{Te}^{*}(r)$ and small $(k_\theta \rho_e)^2$ as:

$$\frac{d^2\tilde{\phi}}{dx^2} - \left(k_\theta^2 - \frac{\left(\frac{k_{//}\upsilon_{Te}}{\omega}\right)^2 \frac{\omega_{Te}}{\omega} + \tau}{\rho_e^2\left(\left(\frac{k_{//}\upsilon_{Te}}{\omega}\right)^2 \frac{\omega_{Te}}{\omega} - 1\right)} \right)\tilde{\phi} = 0 \qquad (1)$$

where $\omega_{Te} = \omega_{Te}(r) = \omega_{Te}^{*}(r) = k_\theta \rho_e \kappa_{Te}(r) \rho_e \Omega_{ce}$, ω_{Te} is the electron temperature gradient diamagnetic drift frequency, $\kappa_{Te}(r) = -d(\ln T_e)/dr$ is inverse temperature scale length and $\tau = T_e/T_i$. Eq.(1) is a Weber type equation and its solution can be described in terms of Hermite polynomials [19] as:

$$\left(\frac{k_{//}\upsilon_{Te}}{\omega_{Te}}\right)^2 + \tau\left(\frac{\omega}{\omega_{Te}}\right)^3 = \left(\frac{k_{//}\upsilon_{Te}}{\omega_{Te}}\right)\left(\frac{\omega}{\omega_{Te}}\right)^{3/2} \sqrt{(\tau+1)\frac{\omega_{Te}^{//}\rho_e^2}{2\omega_{Te}}}\,(2l+1) \qquad (2)$$

where double prime indicates second radial derivative and *l* is the radial mode number. We find a perturbative solution of the above as $\omega = \omega_0 + \delta\omega$, where ω_0 is the local solution and $\delta\omega$ is the non-local correction [19,29]. Then Eq.(2) yields:

$$\frac{\delta\omega}{\omega_{Te}} = \frac{-\sqrt{3}+i}{6\tau^{5/6}}\left(\frac{k_{//}\upsilon_{Te}}{\omega_{Te}}\right)^{2/3}\sqrt{(\tau+1)\frac{\omega''_{Te}\rho_e^2}{2\omega_{Te}}(2l+1)} \qquad (3)$$

For two radial harmonics ω_{12_0} (m=12, l=0) and ω_{12_1} (m=12, l=1), with CLM parameters we obtain $\Delta\omega = \omega_{12\_0} - \omega_{12\_1} \sim 2\pi$ * (30) kHz, which is close to the low frequency third mode of the triad discussed above. This validates the 3-wave coupling interpretation of bicoherency data shown above.

We now discuss in detail the identification of the low frequency mode of the triad discussed above. Its azimuthal mode number m_3 is determined from the set of azimuthal phase shift measured via cross-correlation of two high frequency Langmuir probes [24], displaced azimuthally 90^0 and 180^0 (See Fig.1.) apart to yield $m_3 = 0$. The parallel wavelength is determined from the axial phase shift measured via cross-correlation of two other Langmuir probes, displaced axially by 28.5 cm (See Fig.1.). The resulting phase shift for typical plasma parameters shown in Fig.5. indicates that it is a linear function of frequency in the 30 kHz - 60kHz range. The reciprocal of the slope of this line (See Fig.5.) yields a phase velocity *of* $3.5 \cdot 10^6$*cm/sec* which is in a very good agreement with ion acoustic wave speed $C_s \sim 4 \cdot 10^6$ cm/sec calculated for CLM parameters. Therefore, the low frequency mode in the triad of 3-wave coupling is a plane ion acoustic (IA) mode with $m_3 = 0$ and $\omega_3/2\pi = 45$kHz.

Bicoherence alone is not a proof of a saturation mechanism, it only indicates mode coupling – which is one of the canonical non-linear phenomena in plasma

dynamics [30]. However, if and only if at least one of these modes is damped (ion acoustic mode in our case) mode-coupling will lead to saturation.

We now present another additional experimental evidence of coupling between ETG modes and the low frequency ion acoustic mode. This evidence is based on probing the coupling via feedback diagnostic, which is unique in CLM (See Fig.1.). We use one of the high frequency Langmuir probe [24] as a sensor and an especially designed ring Langmuir probe as an actuator of the feedback circuit (See Fig.1.). We used the ring shape of probe to enhance the efficiency of the actuator and for excitation of plane wave with m=0. The ring probe has a radius of 1.2 cm and wire diameter of 0.2 mm and is placed coaxial with the plasma column. The radius of the ring probe is smaller than the radius where the maximum of ETG mode amplitude is located at 1.8 cm [24]. Its influence in exciting an ETG mode is found to be not significant. The frequency band of the feedback loop was limited by a low pass electronic filter at < 100kHz. We used the ring probe as electrically floating and our feedback signal has an a.c. component only (amplitude $\leq$ 0.1 k*Te/e, phase shift ~ 180^0). Phase and amplitude feedback signal are adjusted by a phase shifter and amplifiers (See feedback circuit in Fig.1.). The results of feedback experiments with different levels of feedback gain shown in Fig.6. indicate that the amplitude of ETG modes (high frequency ~ 2MHz) changed with the changing of the low frequency (~ 45 kHz) mode under feedback control, whereas other plasma parameters remained the same. Therefore, it is a clear demonstration of nonlinear mode coupling between the high frequency modes (ETG) and low frequency mode (IA).

It is noted that in the absence of feedback 3-wave coupling is a closed system. For a closed system, if one mode amplitude goes up another mode must go down. Feedback

opens up the system and allows energy to flow in and out. In this case when one mode goes up in amplitude, another mode may also go up.

A theory of three wave coupling of two ETG harmonics and ion acoustic mode [29] estimated the saturation level of ETG mode about $\varphi_{rms} \sim 10\%$ for CLM parameters which is within the range of the experimental values and not inconsistent with gyrokinetic simulation results for tokamaks. This mode coupling scenario is novel in view of the fact that most mode-coupling theories are restricted to coupling only in azimuthal (poloidal) wave numbers of the same mode, unlike here.

In conclusion the experimental bi-coherence data show coupling between two high frequency (~2MHz) and one low frequency (~45kHz) modes. Measurements of azimuthal wave number (m=0) and parallel wave vector ($k_{//} \approx \omega / C_s$) clear identify that low frequency mode is a plane ion acoustic wave. The theoretical estimation from the non-local dispersion relation for ETG radial harmonics gives difference between the radial harmonics to be about 30kHz, that not far from the frequency of IA mode, indicating multimode interaction. A novel feedback diagnostic independently verified this nonlinear coupling between low frequency mode (IA) and high frequency mode (ETG). It is surmised that this mechanism may be valid for the saturation of all drift waves.

One of the most interesting implications of this study is the near ubiquitous role of damping in collisionless plasmas provided by ion acoustic damping. It may be collisionless analog to viscous damping in classical fluid mechanics.

This research was supported by U.S. Department of Energy Grant No. DE-FG02-98ER-54464.

[1] B. Coppi and G. Rewoldt, in *Advances in Plasma Physics*, edit by A. Simon and W.B. Thompson (Wiley, New York, 1976), Vol. 6, 421.

[2] W. Horton, Rev. Mod. Phys. **71**, 135 (1999).

[3] F.Jenko and W.Dorland, Phys. Rev. Lett. **89**, 225001 (2002).

[4] W. Dorland, F. Jenko, M. Kotschenreuther and B.N. Rogers, Phys. Rev. Lett. **85**, 5579 (2000).

[5] Y. C. Lee, J. Q. Dong, P. N. Guzdar and C. S. Liu, Phys. Fluids **30**, 1331 (1987).

[6] W. Horton, B. G. Hong and W. M. Tang, Phys. Fluids **31** (10), 2971 (1988).

[7] Z. Lin, L. Chen and F. Zonca, Phys. Plasmas **12**, 056125 (2005).

[8] W. Horton, H. V. Wong, P. J. Morrison, A. Wurm, J. H. Kim, J. C. Perez, J. Pratt, G. T. Hoang, B. P. LeBlanc and R. Ball, Nucl. Fusion **45**, 976 (2005).

[9] W. M. Nevins, J. Candy, S. Cowley, T. Dannert, A. Dimits, W. Dorland, C. Estrada-Mila, G. W. Hammett, F. Jenko, M. J. Pueschel and D. E. Shumaker, Phys. Plasmas **13**, 122306 (2006).

[10] R. E. Waltz, J. Candy and M. Fahey, Phys. Plasmas, **14**, 056116 (2007).

[11] A. M. Dimits, W. M. Nevins, D. E. Shumaker, G. W. Hammett, T. Dannert, F. Jenko, M. J. Pueschel, W. Dorland, S. C. Cowley, J. N. Leboeuf, T. L. Rhodes, J. Candy and C. Estrada-Mila, Nucl. Fusion **47,** 817 (2007).

[12] U.Zakir, Q.Haque, and Qamar, Phys. Plasmas **20**, 052106 (2013).

[13] L. Schmitz, A. E. White, T. A. Carter, W. A. Peebles, T. L. Rhodes, W. Solomon and K. H. Burrell, Phys. Rev. Lett. **100**, 035002 (2008).

[14] E. Mazzucato, D. R. Smith, R. E. Bell, S. M. Kaye, J. C. Hosea, B. P. LeBlanc, J. R. Wilson, P. M. Ryan, C. W. Domier, N. C. Luhmann, Jr., H. Yuh, W. Lee and H. Park, Phys. Rev. Lett. **101**, 075001 (2008).

[15] E. Z. Gusakov, A. D. Gurchenko, A. B. Altukhov, A. Yu. Stepanov, L. A. Esipov, M. Yu. Kantor and D. V. Kouprienko, Plasma Phys. Control. Fusion **48**, A371 (2006).

[16] C.Moon, T.Kaneko, and R.Hatakeyama, Phys.Rev.Lett.**111**, 115001 (2013).

[17] V.Sokolov, and A.K. Sen, Phys. Rev. Lett. **92**, 165002 (2004).

[18] V.Sokolov and A.K.Sen, Nucl. Fusion **45,** 439 (2005).

[19] S.E. Parker and A.K. Sen, Phys. Plasmas **9,** 3440 (2002).

[20] P.H. Diamond, S-I Itoh, K.Itoh and T.S.Hahm, Plasma Phys.Controlled Fusion **47**, R35 (2005).

[21] V.Sokolov, X.Wei, A.K. Sen, and K. Avinash, Plasma Phys.Controlled Fusion **48**, S111 (2006).

[22] V.Sokolov, and A.K. Sen, Phys. Rev. Lett. **104**, 025002 (2010).

[23] R. Scarmozzino, A. K. Sen and G. A. Navratil, Phys. Fluids **31**, 1773 (1988).

[24] X.Wei, V.Sokolov, and A.K. Sen, Phys. Plasmas **17**, 042108 (2010).

[25] X.R. Fu, W. Horton, Y. Xiao, Z. Lin, A.K. Sen, and V. Sokolov, Phys. Plasmas **19,** 032303 (2012).

[26] V.Sokolov, and A.K. Sen, Phys. Rev. Lett. **107**, 155001 (2011).

[27] Y.C. Kim and E.J.Powers, IEEE Trans. Plasma Sci. **7,** 120 (1979).

[28] R.J. Goldston, and P.H. Rutherford, *Introduction to Plasma Physics*, Taylor & Francis Group, LLC, New York, 1995.

[29] E.K.Tokluoglu, V.Sokolov and A.K.Sen, Phys. Plasmas **19**, 102306 (2012).

[30] R.Z.Sagdeev, and A.A.Galeev, *Nonlinear Plasma Theory, W.A.*Benjamin, Inc. New York, 1969.

Fig. 1. (Color online) Scheme of CLM and diagnostic setup.

Fig. 2. (Color online) Power Spectra of potential fluctuation .

Fig. 3. (Color online) The bicoherence of ETG mode coupling, frequency units are kHz.

(a) Bicoherence and corresponding power spectrum

(b) A close-up of the bicoherence

Fig. 4. (Color online) Radial profiles of electron temperature and inverse scale length

$1/L_{Te} = - d(\ln Te)/dr$

Fig. 5. (Color online) Measurement of the parallel phase velocity of the low frequency mode. The dash line is power spectrum, the solid line is phase shift between two axial probes.

Fig. 6. (Color online) The power spectra of potential fluctuations vs different levels of feedback gain. The "Strong" level corresponds to ~0.1 k*Te/e and the "Weak" level is about 0.03 k*Te/e

(a) Low frequency part (IA mode)

(b) High frequency part (ETG mode)

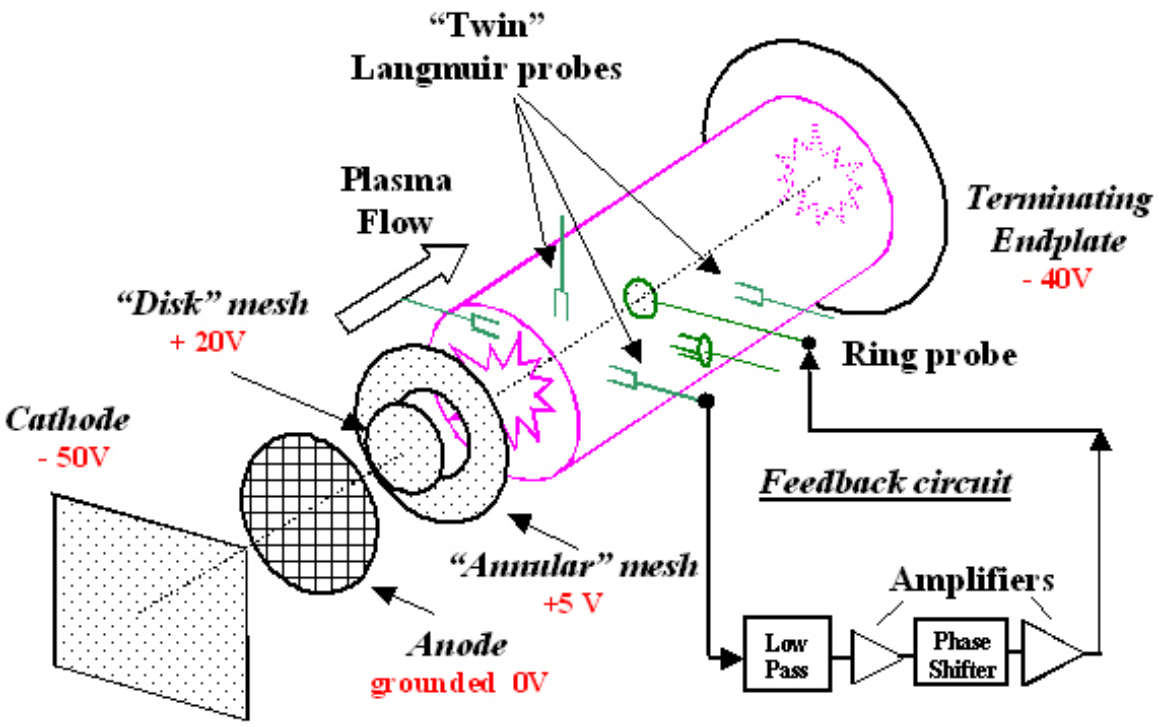
"Twin"
Langmuir probes
Plasma
Flow
Terminating
Endplate
- 40V
"Disk" mesh
+ 20V
Ring probe
Cathode
- 50V
Feedback circuit
"Annular" mesh
+5 V
Amplifiers
Anode
grounded 0V
Low
Pass
Phase
Shifter

Fig.1.

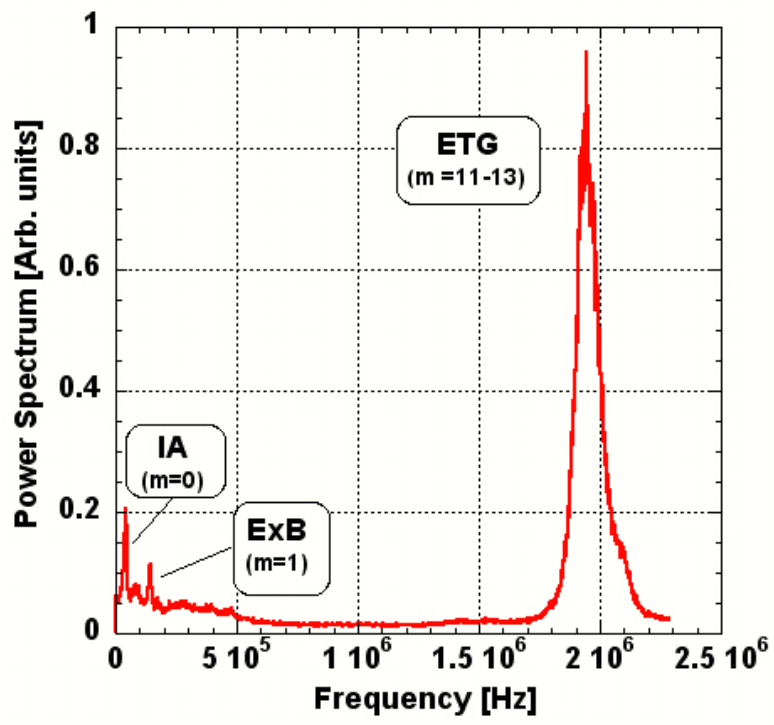
Power Spectrum [Arb. units]
Frequency [Hz]
ETG
(m =11-13)
IA
(m=0)
ExB
(m=1)
0
0.2
0.4
0.6
0.8
1
0
5 10^5
1 10^6
1.5 10^6
2 10^6
2.5 10^6

Fig.2.

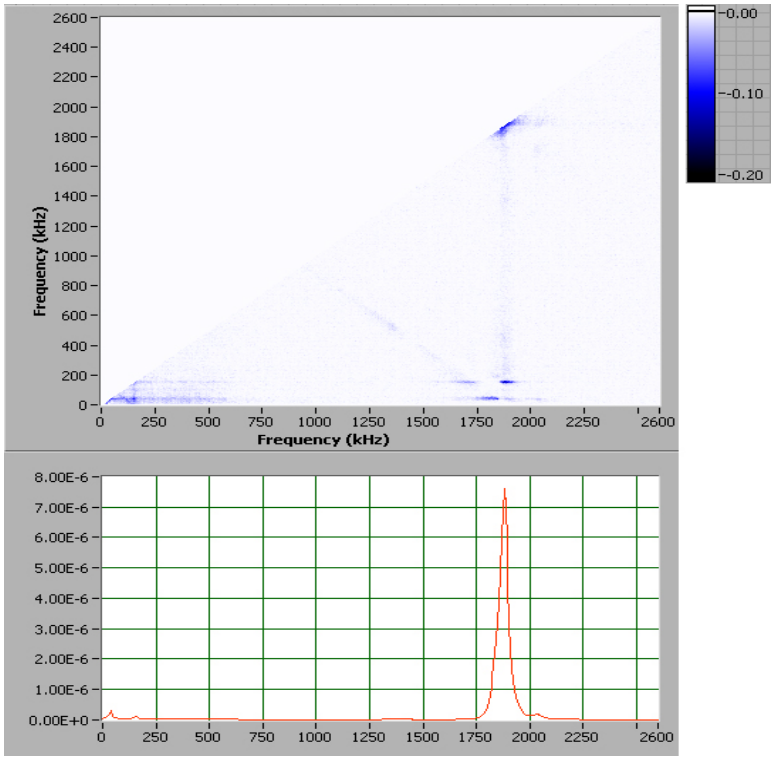
Frequency (kHz)
Frequency (kHz)
-0.00
--0.10
--0.20

Fig 3 a)

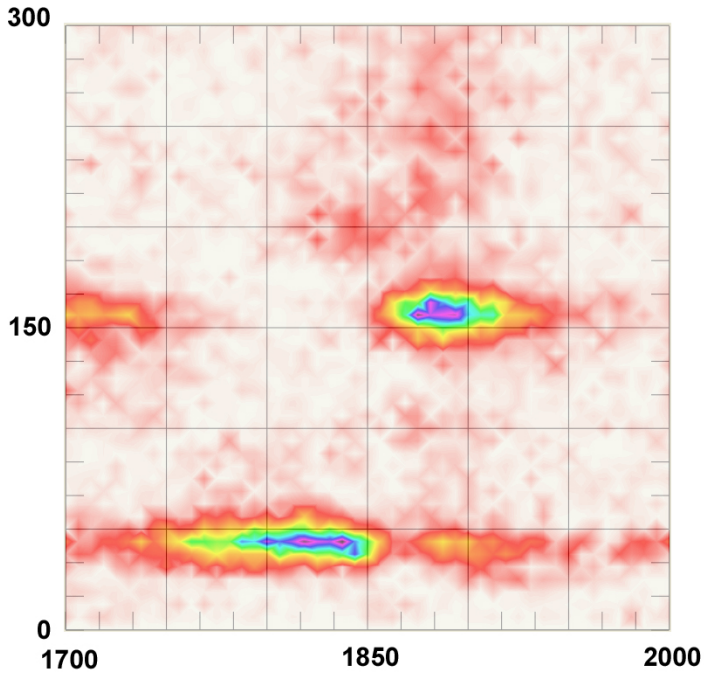
300
150
0
1700
1850
2000

Fig 3 b)

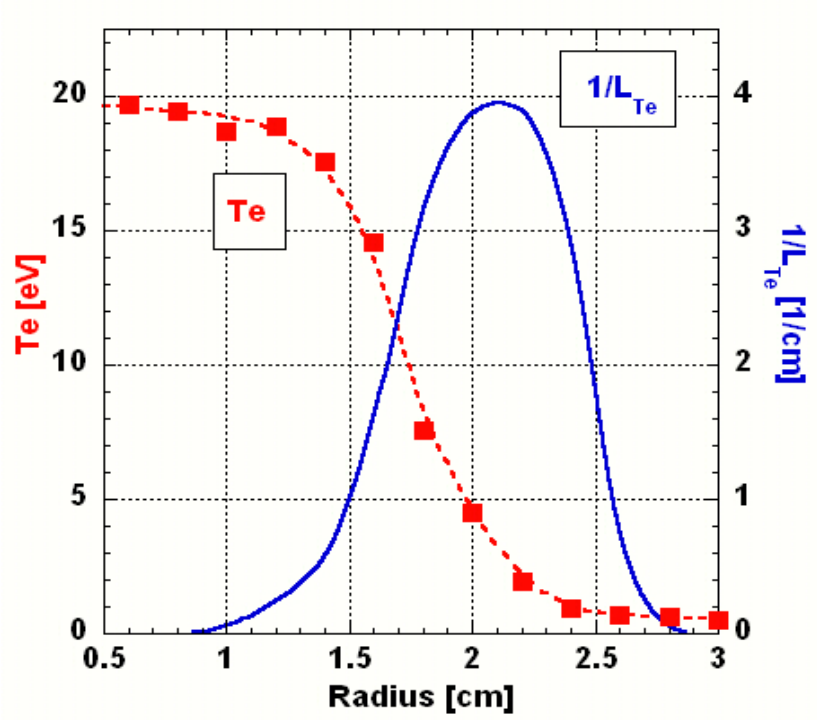
1/L_Te
Te
Te [eV]
1/L_Te [1/cm]
Radius [cm]
20
15
10
5
0
4
3
2
1
0
0.5
1
1.5
2
2.5
3

Fig. 4.

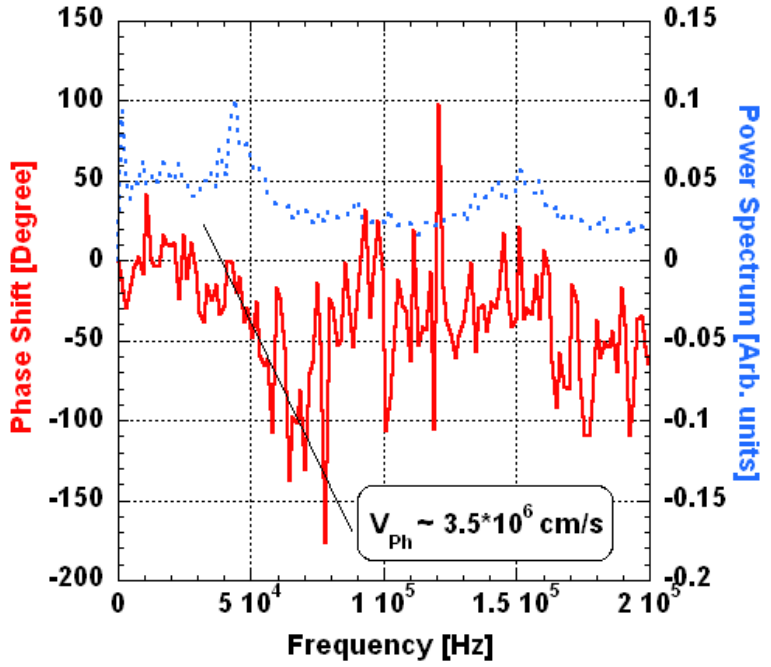
Phase Shift [Degree]
Power Spectrum [Arb. units]
Frequency [Hz]
V_Ph ~ 3.5*10^6 cm/s
150
100
50
0
-50
-100
-150
-200
0.15
0.1
0.05
0
-0.05
-0.1
-0.15
-0.2
0
5 10^4
1 10^5
1.5 10^5
2 10^5

Fig.5.

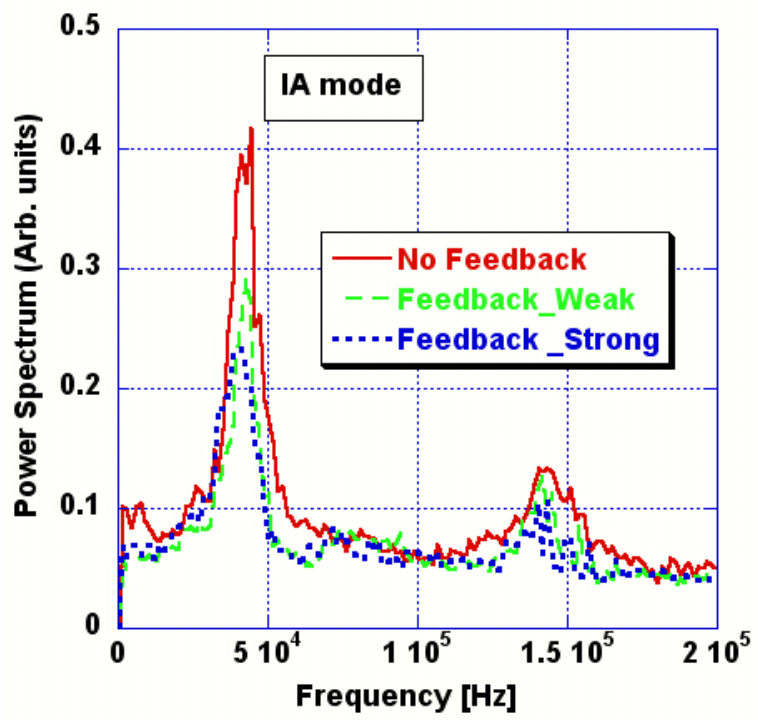
IA mode
No Feedback
Feedback_Weak
Feedback _Strong
Power Spectrum (Arb. units)
Frequency [Hz]
0.5
0.4
0.3
0.2
0.1
0
0
5 10^4
1 10^5
1.5 10^5
2 10^5

Fig. 6. a)

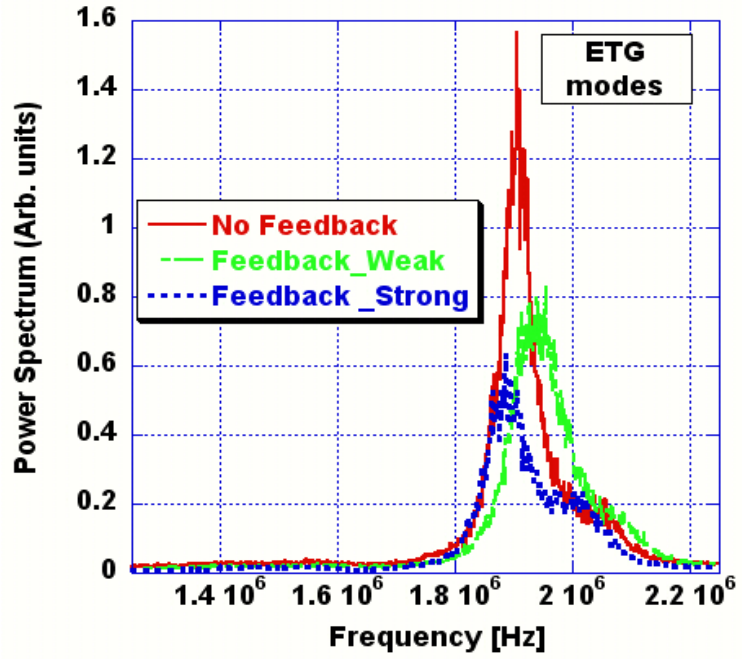
ETG modes
No Feedback
Feedback_Weak
Feedback _Strong
Power Spectrum (Arb. units)
Frequency [Hz]
1.6
1.4
1.2
1
0.8
0.6
0.4
0.2
0
1.4 10^6
1.6 10^6
1.8 10^6
2 10^6
2.2 10^6

Fig.6. b)